Hirose and Kobayashi
Earth, Planets and Space (2025) 77:18
https://doi.org/10.1186/s40623-025-02145-5

Earth, Planets and Space

FULL PAPER **Open Access**

Tidal correlation of deep tectonic tremors increases during long-term slow slip events in the Bungo Channel, southwest Japan

Fuyuki Hirose[1*] and Akio Kobayashi[2]

Abstract

In the Bungo Channel along the Nankai Trough, southwest Japan, long-term slow slip events (LSSEs) of about M_W 6–7 and lasting 6–12 months occur at several-year intervals at the base of the seismogenic zone. In sync with these LSSEs, deep tectonic tremors are activated at the base of the LSSE zone. The tidal response of tectonic tremors during short-term slow slip events lasting several days has been extensively investigated, but variations of the tidal correlation of tectonic tremors over periods on the order of years remain poorly understood. Here, we investigated long-term temporal changes in the correlation between deep tectonic tremors and tides in the Bungo Channel. We found that tectonic tremors along the base of the LSSE region (region Ba) are strongly correlated with tidal shear stress and/or Coulomb failure stress under a very small apparent friction coefficient, and that these tremors are more likely to occur when the tidal stress acting in the direction promoting fault slip is large. We also found that tidal sensitivity is relatively high during LSSE periods and low during other periods. Because the LSSE region largely includes region Ba, fault coupling in region Ba during LSSE periods is undoubtedly smaller than during other periods. As a result of this low friction state, even tidal stresses much smaller than the lithostatic stress can affect the generation of deep tectonic tremor, and tidal sensitivity during LSSE periods seems to be higher than during other periods.

Keywords Tide, Deep tremors, Long-term slow slip, Bungo Channel

*Correspondence:
Fuyuki Hirose
fhirose@mri-jma.go.jp
Full list of author information is available at the end of the article

Graphical abstract

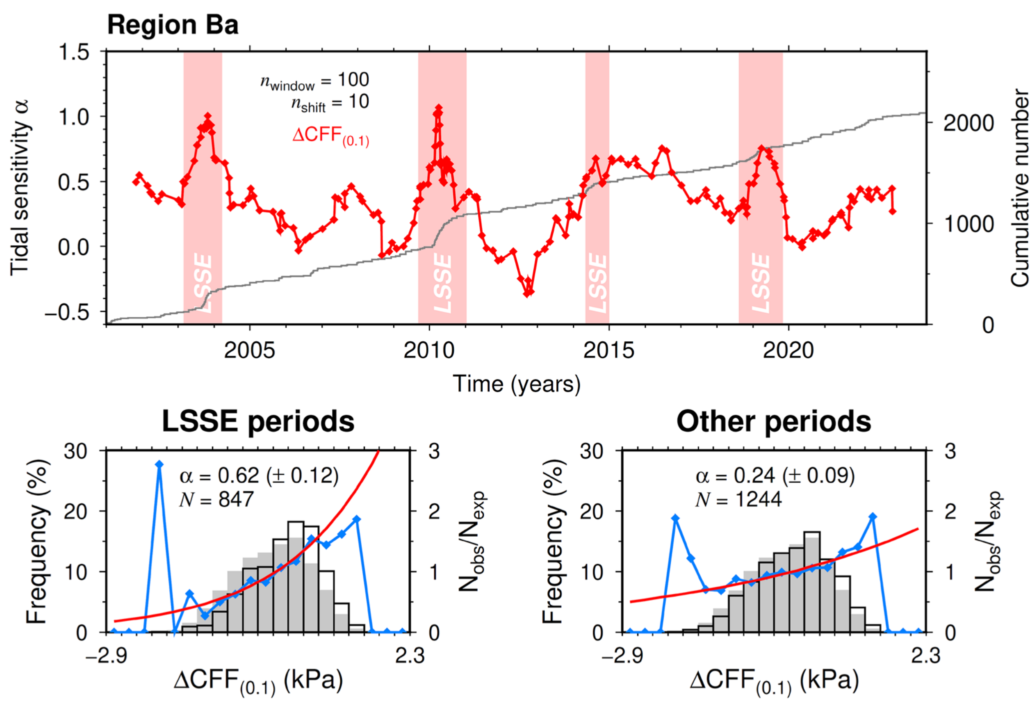

1 Introduction

Over the past 30 years, slow earthquakes have been detected in many regions around the Pacific Rim (Obara and Kato 2016). Slow earthquakes are characterized by long-term slow slip events (LSSEs) lasting several months to years, short-term slow slip events (SSSEs) lasting several days to weeks, and tectonic tremor (TT) and low-frequency earthquakes with dominant frequencies of a few Hz. TT and SSSEs are often synchronized; therefore the two are collectively called episodic tremor and slip (ETS) (Rogers and Dragert 2003).

Tectonic tremor tends to be highly correlated with tidal shear stress or Coulomb stress with a very small friction coefficient (e.g., Thomas et al. 2009; Houston 2015). In this case, TT is affected by the phase (especially the semidiurnal period; e.g., Ide 2010, 2012; Katakami et al. 2017) and/or the amplitude of the tidal stress (e.g., Lambert et al. 2009; Houston 2015; Ide et al. 2015). Because tidal stress, which is much smaller than lithostatic stress, affects the occurrence of TT, the faults in the TT occurrence area are hypothesized to be very weak (low friction; e.g., Rubinstein et al. 2008; Thomas et al. 2009; Houston 2015). Thus, the tidal correlation of TT may be applied to elucidate the coupling state of the plate boundary. The tidal response of TT during ETS lasting several days has been extensively studied; however, we are not aware of any studies that have focused on variations in the tidal correlation of TT over periods on the order of years.

In southwest Japan, where the Philippine Sea plate is subducting beneath the continental plate along the Nankai Trough, great earthquakes of moment magnitude (M_w) 8–9 occur at intervals of about 100 years (Earthquake Research Committee 2013). In the Bungo Channel along the Nankai Trough (Fig. 1), LSSEs of M_w 6–7 lasting about one year occur repeatedly at intervals of several years at the base of the seismogenic zone (e.g., Kobayashi 2017; Ozawa 2017; Takagi et al. 2019); TT activity is synchronized with these LSSEs (Hirose et al. 2010). Hereinafter, TT occurring at the base of the seismogenic zone is called deep tectonic tremor (DTT). DTTs are distributed along the 30 km depth contour for the top of the subducting Philippine Sea plate along the Nankai Trough (Obara 2002, 2010) (Fig. 1a). SSSEs of M_w 5–6 are often synchronized spatially and temporally with the DTT region (Obara 2010) (Fig. 1a). In this study, we investigated long-term temporal changes in the correlation between DTT and tides in the Bungo Channel.

2 Data

2.1 Characteristics of DTT

In this study, we used the DTT catalog of the National Research Institute for Earth Science and Disaster Resilience (NIED) (Maeda and Obara 2009; Obara et al. 2010; https://hinetwww11.bosai.go.jp/auth/tremor/auto_hypo_catalog), which comprises events detected by the envelope correlation method. This DTT catalog consists of tremor data objectively detected using the same method over a long time period, making it suitable for the purpose of this study, which is to investigate the long-term temporal changes in the correlation between DTT and tides. The data used in this study were DTTs in regions Ba and Bb beneath the Bungo Channel from 1 January 2001 to 31 October 2023 (2091 and 2659 events, respectively; Fig. 1b). Regions Ba and Bb were defined according to Obara et al. (2010), who delineated the regions based on the bimodal characteristics of the dip direction of the TT distribution. DTTs in region Ba increased during LSSE periods (Fig. 2). In particular, the increase in the number of DTTs was remarkable during the four periods in which the baseline length between Global Navigation Satellite System (GNSS) stations 950,449 and 940,079 changed rapidly (highlighted in pink in Fig. 2; see Fig. 1a for location). In contrast, DTTs occurred regularly in region Bb; their frequency of occurrence has increased since around 2019, but this increase may be due to artificial noise rather than TT (National Research Institute for Earth Science and Disaster Resilience 2019). We do not consider the increase in DTTs in region Bb in detail in this study, but we note that the epicenters during that period were clustered in the southwest part of region Bb (letter "A" in Fig. 1b). Figure 3 shows histograms of the occurrence intervals of DTTs. The time resolution of the DTT catalog is 1 h. Because most DTTs occur with an occurrence interval of a few hours, DTTs tend to occur almost continuously. Quiet periods of several tens of days occur occasionally; these quiet periods are longer in region Ba than in region Bb (cf. Figure 3d and h).

2.2 Fault parameters

Calculation of the theoretical tidal response to a DTT requires information on the location, occurrence time, and fault parameters of the DTT. Figure 4 shows the epicenters and fault parameters of the studied DTTs. For the DTT locations, epicenters were taken directly from the catalog. Because the DTT catalog does not contain depth information, it was assumed that the DTT occurred at the plate boundary (Hirose et al. 2008). Catalog values were used directly for occurrence times, i.e., the time resolution is 1 h, so it was assumed that the DTTs occurred on the hour. In addition to direct triggering of DTT by tides, the possibility of secondary DTT contamination trigged by preceding DTT cannot be denied, but we have no idea to properly separate them. In this study, we deal with binary information, i.e., whether an DTT occurred (1) or did not occur (0) within a 1-h bin in a region, which means that we used a declustered dataset in a sense. Information on the strike and dip angles of the DTTs were not available; hence, these values were estimated from the plate configuration (more specifically, the maximum dip direction was calculated from depth contours, and the direction perpendicular to it was taken as the strike). For simplicity, the rake angle was taken as the angle between the direction of motion of the continental plate relative to the Philippine Sea plate (N124°E) (DeMets et al. 2010) and the strike angle of each DTT.

2.3 Spatiotemporal distribution of LSSEs

During the analysis period, LSSEs occurred multiple times in the Bungo Channel. The area and period of these LSSEs differed depending on the researcher and analysis method (e.g., Kobayashi 2017; Nakata et al. 2017; Ozawa 2017; Takagi et al. 2019). For the LSSE slip distribution, analyses have been conducted under the assumption of a smooth slip distribution to compensate for the lack of crustal deformation observational data. In contrast, Nakata et al. (2017) estimated the detailed LSSE slip distribution using a sparse modeling method that enabled

(See figure on next page.)

Fig. 1 Maps of the region around the Bungo Channel, southwestern Japan. **a** Regional map (inset) showing the location of the study area (red rectangle); the arrow indicates the direction of movement of the Philippine Sea plate (PHS) relative to the Amur continental plate (AM) (DeMets et al. 2010), NT indicates the Nankai Trough, PAC indicates the Pacific plate, and OK indicates the Okhotsk plate. The main map shows the relationship of the Bungo Channel to the Nankai Trough, the postulated tsunamigenic area of Nankai megathrust earthquakes (shaded green; Central Disaster Management Council 2003), epicenters of DTTs that occurred between January 2001 and October 2023 (red dots; Maeda and Obara 2009; Obara et al. 2010), and areas of SSSEs from June 1996 through January 2012 (orange rectangles; Nishimura et al. 2013). The purple shaded area indicates areas with slip ≥ 0.2 m, and the purple outlines mark 0.1-m contours of the 2010 LSSE (Nakata et al. 2017). Numbered green squares are the locations of Global Navigation Satellite System (GNSS) stations. Dashed blue lines are depth contours of the top of the subducting Philippine Sea plate (Hirose et al. 2008; Nakajima and Hasegawa 2007). **b** Enlarged view of the rectangular area in the main map of panel **a**. The regions labeled Ba and Bb were defined by Obara et al. (2010). The focal mechanism of a deep very-low-frequency earthquake (Ide and Yabe 2014) is shown in lower-hemisphere equal-area projection. The cluster "A" in region Bb is explained in Sect. 2.1

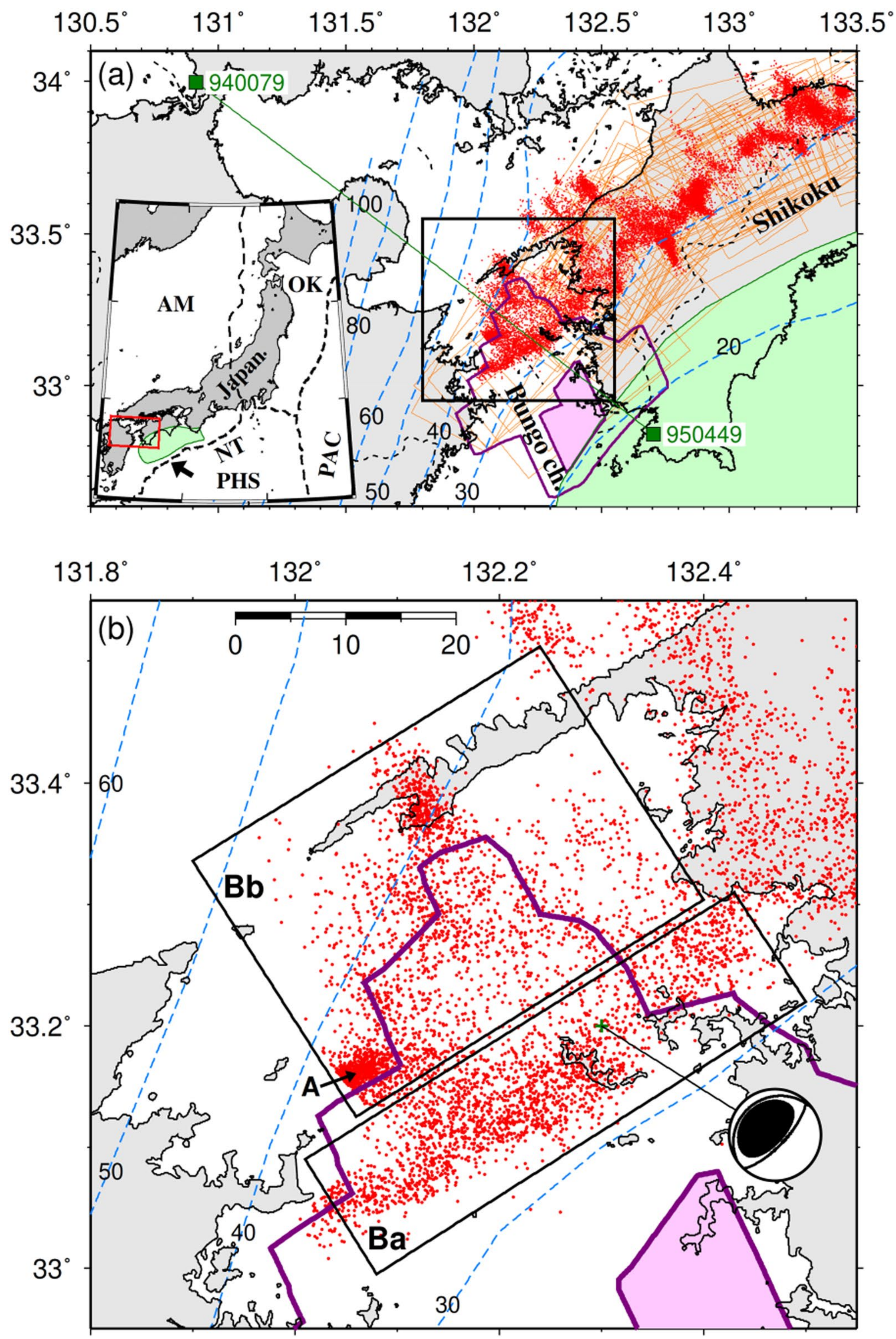

Fig. 1 (See legend on previous page.)

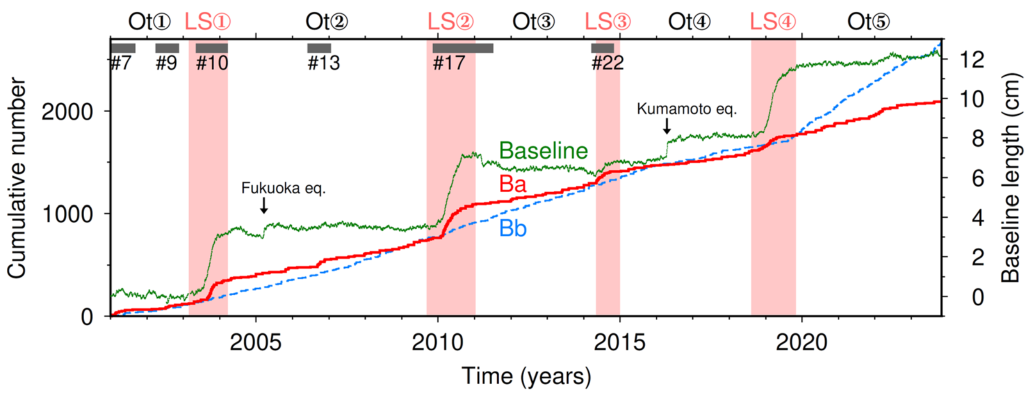

Fig. 2 Cumulative number of DTTs in the study area during 2001–2023. Red and blue curves (left axis) show the cumulative number of DTTs in regions Ba and Bb, respectively. The green curve (right axis) shows the 11-day moving median of the change of the detrended baseline length between GNSS stations 950,449 and 940,079 during January 2001 to October 2023. Pink shaded areas highlight periods of LSSE activity determined using the method of Kobayashi (2017; see Fig. 5). The numbered gray bars at the top of the diagram indicate periods of LSSE activity estimated by Takagi et al. (2019). LS indicates an LSSE period; Ot indicates a period that was not an LSSE

accurate extraction of necessary information from insufficient crustal deformation data (purple shaded area and purple contour in Fig. 1). They detected abrupt changes in slip amount at the updip and downdip ends of the major slip area (purple shaded area in Fig. 1), the former coinciding well with the lower limit of the seismogenic zone and the 350 °C isotherm, and the latter coinciding well with the updip limit of the DTT zone. Kobayashi (2017) developed a method to objectively detect LSSEs by correlation between displacement of GNSS and ramp function. In the present study, the start and end times of LSSEs were defined as the periods when the correlation coefficient obtained by the method of Kobayashi (2017) was 0.8 or more at the center (132.4°E) of the LSSE recognized by Nakata et al. (2017) (Fig. 5). When applied to the F5 solution of the GNSS data, four periods met this condition:

1. 23 February 2003 to 22 March 2004;
2. 10 September 2009 to 9 January 2011;
3. 5 May 2014 to 31 December 2014;
4. 9 August 2018 to 30 October 2019.

These periods are highlighted in pink in Fig. 2. LSSE magnitudes were ~ 7 in periods 1, 2, and 4, and 6.2 in period 3 (Ozawa 2017; Ozawa et al. 2020). The gray bars at the top of Fig. 2 are LSSEs that occurred near the Bungo Channel, as identified by Takagi et al. (2019); LSSEs #10, 17, and 22 were also estimated by Kobayashi (2017)'s method as LSSEs 1–3. Three additional occurrences (#7, #9, and #13) were identified (Fig. 6). The DTTs in region Ba also tended to increase during LSSEs #7, #9, and #13, but by much less than during LSSEs 1–4 estimated by the method of Kobayashi (2017), and the change in the GNSS baseline length was also smaller during LSSEs #7, #9, and #13 (Fig. 2).

3 Method

3.1 Theoretical tidal response

We calculated theoretical tidal responses on the faults using the "TidalStrain.2" Fortran software (Hirose et al. 2019). We investigated changes in the following 12 components as tidal indices: volume strain ΔV at the hypocenter; shear stress $\Delta\tau$; normal stress $\Delta\sigma$; and the Coulomb failure function $\Delta CFF = \Delta\tau + \mu\prime\Delta\sigma$ for assumed apparent friction coefficients $\mu\prime$ of 0.1, 0.2, ..., 0.9 (denoted $\Delta CFF_{(0.1)}$, $\Delta CFF_{(0.2)}$, ..., $\Delta CFF_{(0.9)}$, respectively) on the assumed fault plane. If a highly anisotropic fault hosted fluid-filled fractures aligned along the fault zone, then $\mu\prime = \mu_0(1 - B)$ (Houston 2015), where μ_0 is the static friction coefficient and B is Skempton's coefficient, which indicates the ratio of the change in pore fluid pressure to the change in confining pressure acting on the rock under undrained conditions. Accordingly, if the response of pore pressure to $\Delta\sigma$ is strong (i.e., $B \approx 1$) on the fault plane, $\mu\prime$ becomes small. For details of the method, see Hirose et al. (2019).

In the case of ΔV and $\Delta\sigma$, we defined expansion/dilatation as positive and contraction/compression as negative, and we defined $\Delta\tau$ and ΔCFF as positive when they promoted fault slip. When considering reverse fault-type slip, as in this region, the direction of normal stress that promotes fault slip corresponds to positive.

3.2 Tidal sensitivity

We investigated whether the timing of DTT occurrence is related to tidal values (amplitude). An example analysis is illustrated in Fig. 7. To evaluate whether the likelihood

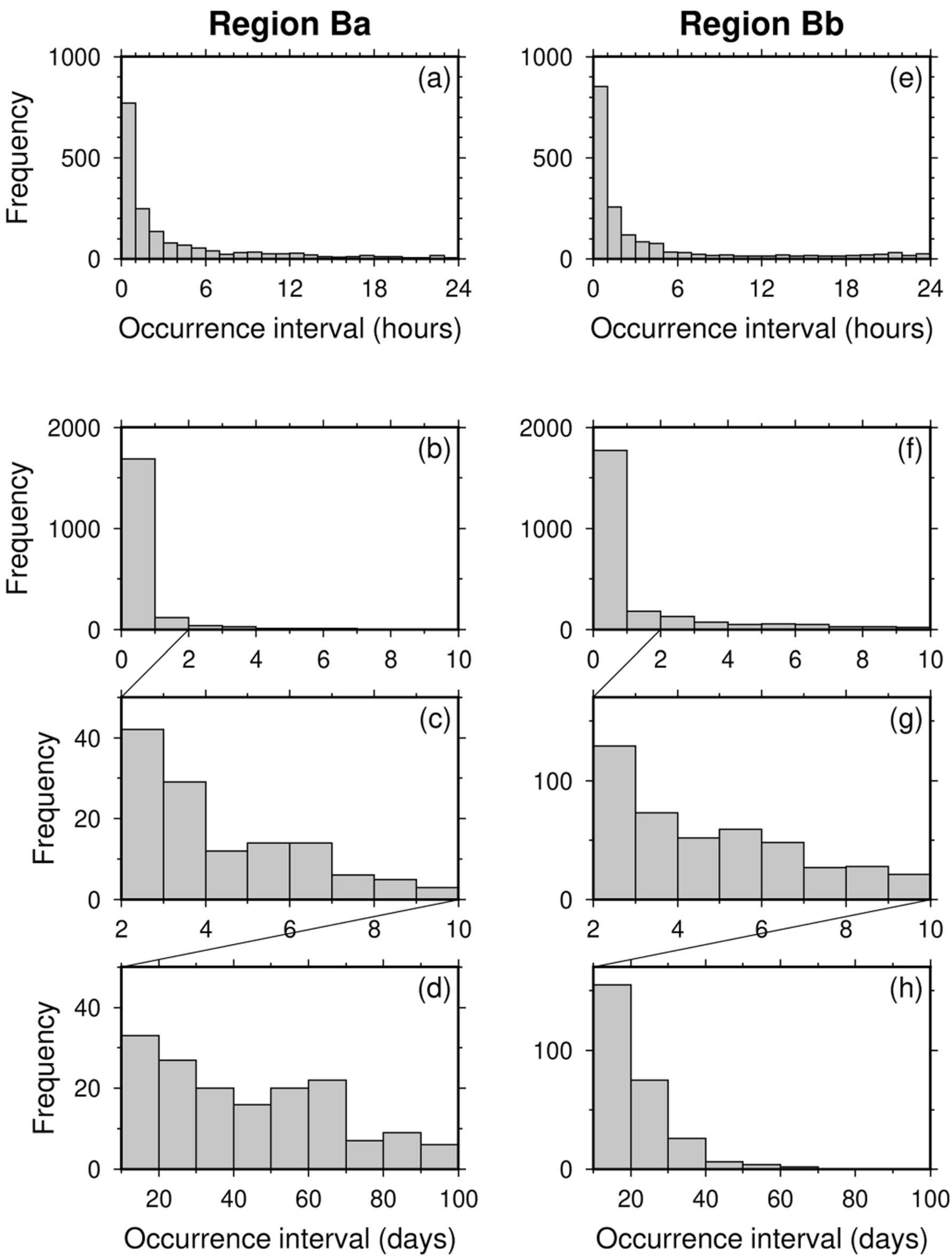

Fig. 3 Frequency distribution of the occurrence intervals of DTTs in regions (left) Ba and (right) Bb. The units of the horizontal axes in **a**, **e** are hours, and the units of the horizontal axes in other panels are days. Note that the vertical axes in **c**, **d** and **g**, **h** are at different scales

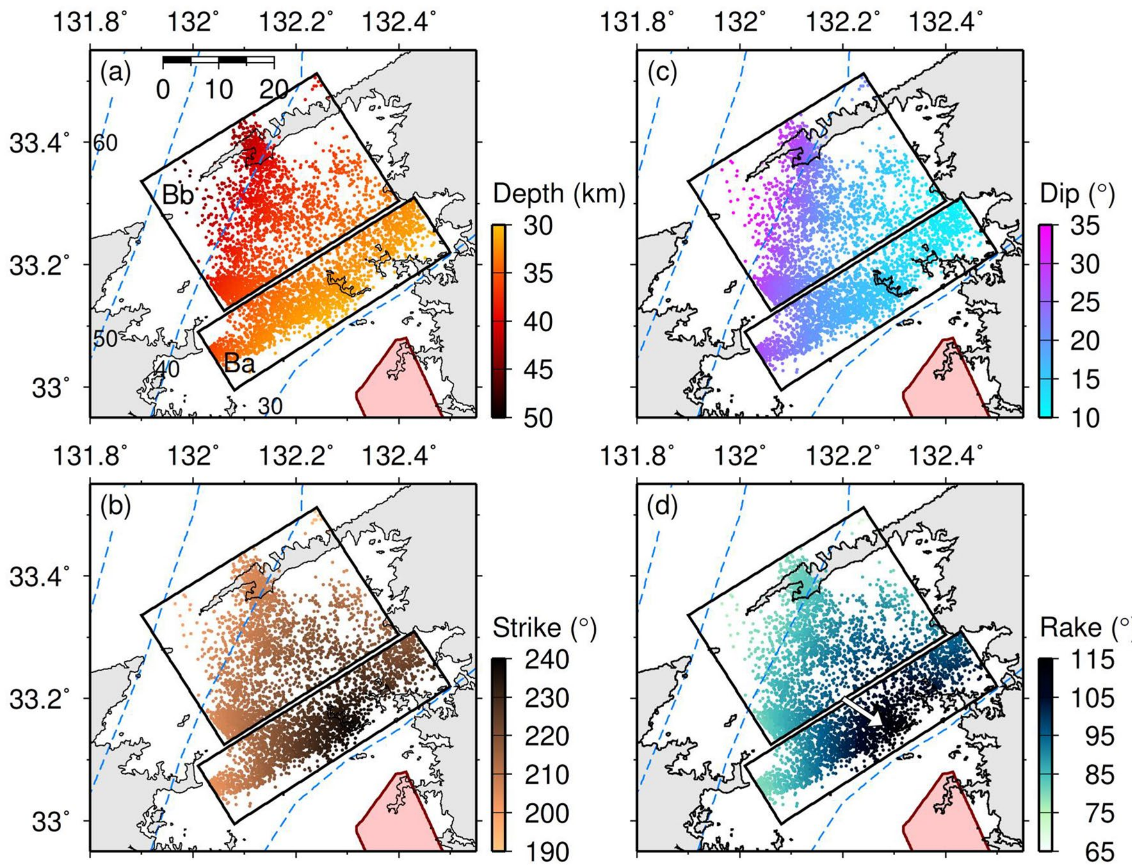

Fig. 4 Distributions of DTT fault parameters. **a** Focal depth, **b** strike, **c** dip, and **d** rake. The arrow in d indicates the direction of movement of the continental plate relative to the Philippine Sea plate (DeMets et al. 2010). Other symbols are as in Fig. 1

of an earthquake increases as the tidal level increases, we used the following formula (Houston 2015) to evaluate the case in which tidal value is subdivided into multiple bins:

$$N_{\mathrm{obs}}(\Delta S)/N_{\mathrm{exp}}(\Delta S) = e^{\alpha \Delta S}, \quad (1)$$

where ΔS is the center value in a strain or stress bin, and the tidal sensitivity α is estimated by the maximum likelihood method (Yabe et al. 2015). The larger the value of α, the greater the tidal sensitivity. The units of α in this study are $/10^{-8}$ for strain and /kPa for stress. N_{obs} is the number of DTTs observed during the period when the tidal force takes the value within the strain/stress bin. N_{exp} is the expected number of DTTs during the same period if there were no correlation to tides, based on 15-min samplings of tidal forces over the 4 days before and after each DTT occurrence (referred to as background data). This is because the tidal response for the fault of each DTT are different due to the different hypocenter and fault parameters of each DTT as shown in Fig. 4. In other words, background data are created from 769 data (=60 min / 15 min × 24 h × 8 days + 1) per DTT, and stacked as many times as there are DTTs. Figure 7 shows an image after stacking. A tidal association would be suggested if $N_{\mathrm{obs}}/N_{\mathrm{exp}}$ (blue diamonds in Fig. 7b) is exponentially proportional to the tidal values. The uncertainty on α, $\Delta\alpha$, was estimated as $2\left|\frac{\partial^2 \ln L}{\partial \alpha^2}\right|^{-1/2}$, which corresponds to the 95% confidence interval of a Gaussian distribution (see Equation [7] in Yabe et al. 2015), where $\ln L$ is the log-likelihood.

4 Results and discussion

4.1 Tidal dependence of DTT

The tidal sensitivity of each tidal component in region Ba is shown in Fig. 8. Each component is normalized by the minimum and maximum values of the background data. Note that $N_{\mathrm{obs}}/N_{\mathrm{exp}}$ outliers in bins near both extremes of the distribution appear due to a lack of data. As the apparent friction coefficient μ' becomes smaller (i.e., as the contribution of $\Delta\sigma$ becomes smaller and the contribution of $\Delta\tau$ becomes larger), the tidal sensitivity tends to increase. The tidal sensitivity α reaches a maximum

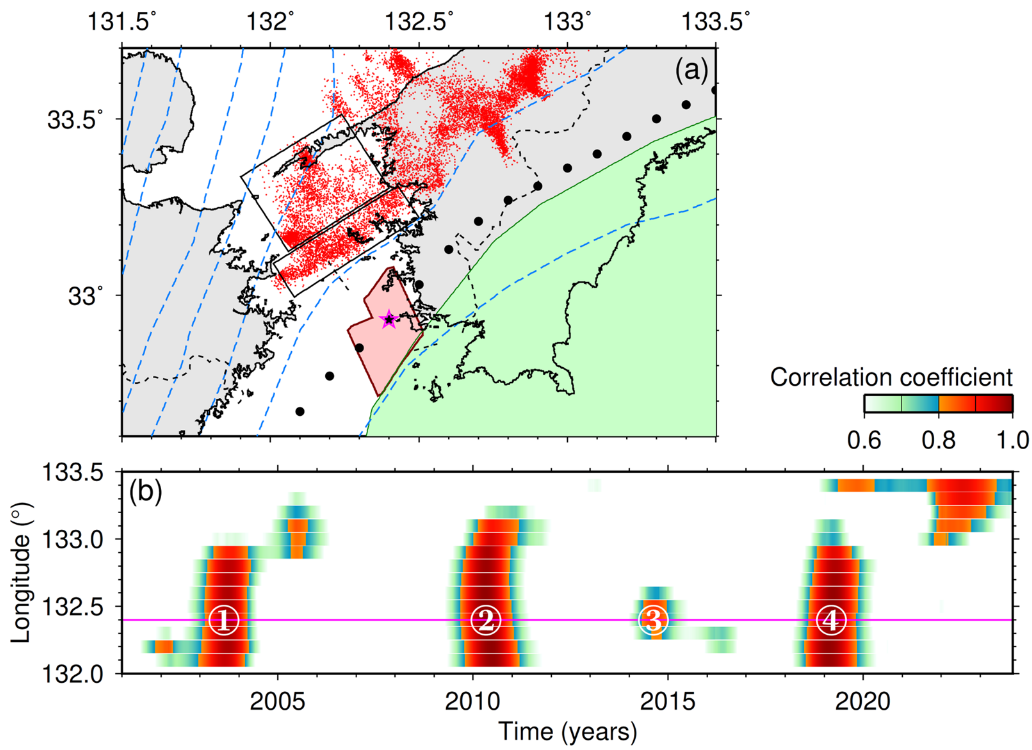

Fig. 5 Four periods of LSSE activity identified by applying the method of Kobayashi (2017). **a** Map showing 15 locations where the top of the Philippine Sea plate is at ~ 25 km depth (black dots). The star marks the location of longitude 132.4°E. Dashed blue lines are depth contours to the top of the Philippine Sea plate. **b** Time vs. longitude plot showing the correlation coefficient between the ramp function and average displacement within 100 km × 50 km rectangles centered on the dots in panel **a**. Colored regions have correlation coefficients > 0.6 and 2-year displacements > 2 mm. Other symbols are as in Fig. 1

of ~ 0.4 for $\Delta \mathrm{CFF}_{(0.1)}$ and $\Delta\tau$, which is significant even considering the uncertainty $\Delta\alpha = 0.07$, suggesting that a DTT is more likely to occur or be suppressed as the absolute value of the tidal force increases. This finding is consistent with previous studies indicating that TT tends to show a high correlation with tidal shear stress or Coulomb stress when the apparent friction coefficient is very small (e.g., Thomas et al. 2009; Houston 2015). Because the apparent friction coefficient should be very small, the response of pore fluid pressure to $\Delta\sigma$ on the fault plane should be strong. The tidal sensitivity of each tidal component in region Bb is shown in Fig. 9. Here, we show the results using data up to December 2017, which are considered to be free from the influence of artificial noise (see Sect. 2.1). As in region Ba, the tidal sensitivity is higher in $\Delta\tau$ and $\Delta \mathrm{CFF}_{(0.1)}$, but the tidal sensitivity is smaller than that in region Ba. If all data up to October 2023 were used, the tidal sensitivity was almost zero for all components.

Indeed, Ide (2010) showed that the tidal sensitivity of DTTs is higher on the updip side (region Ba) than on the downdip side (region Bb). They found that isolated short-duration DTTs, such as low-frequency earthquakes, are more prevalent on the updip side and more sensitive to tides, whereas DTTs on the downdip side show characteristics of diffusive propagation, have longer durations, and are less sensitive to tides. Regarding the difference in tidal sensitivity between shallow and deep tremors, Yabe et al. (2015) considered a collection of velocity-weakening tremor patches embedded in a velocity-strengthening

(See figure on next page.)

Fig. 6 Distribution of LSSEs in the Bungo Channel region. Blue rectangles indicate LSSE faults estimated by Takagi et al. (2019). Blue arrows indicate the slip direction of the upper (Amur) plate and the length of the arrows indicate relative amounts of slip. Event numbers from Takagi et al. (2019), start and end dates (YYYY/MM/DD) of slip, moment magnitude, and amount of slip are listed at the top left of each panel. Red dots are DTTs that occurred within the period of each panel. Other symbols are as in Fig. 1

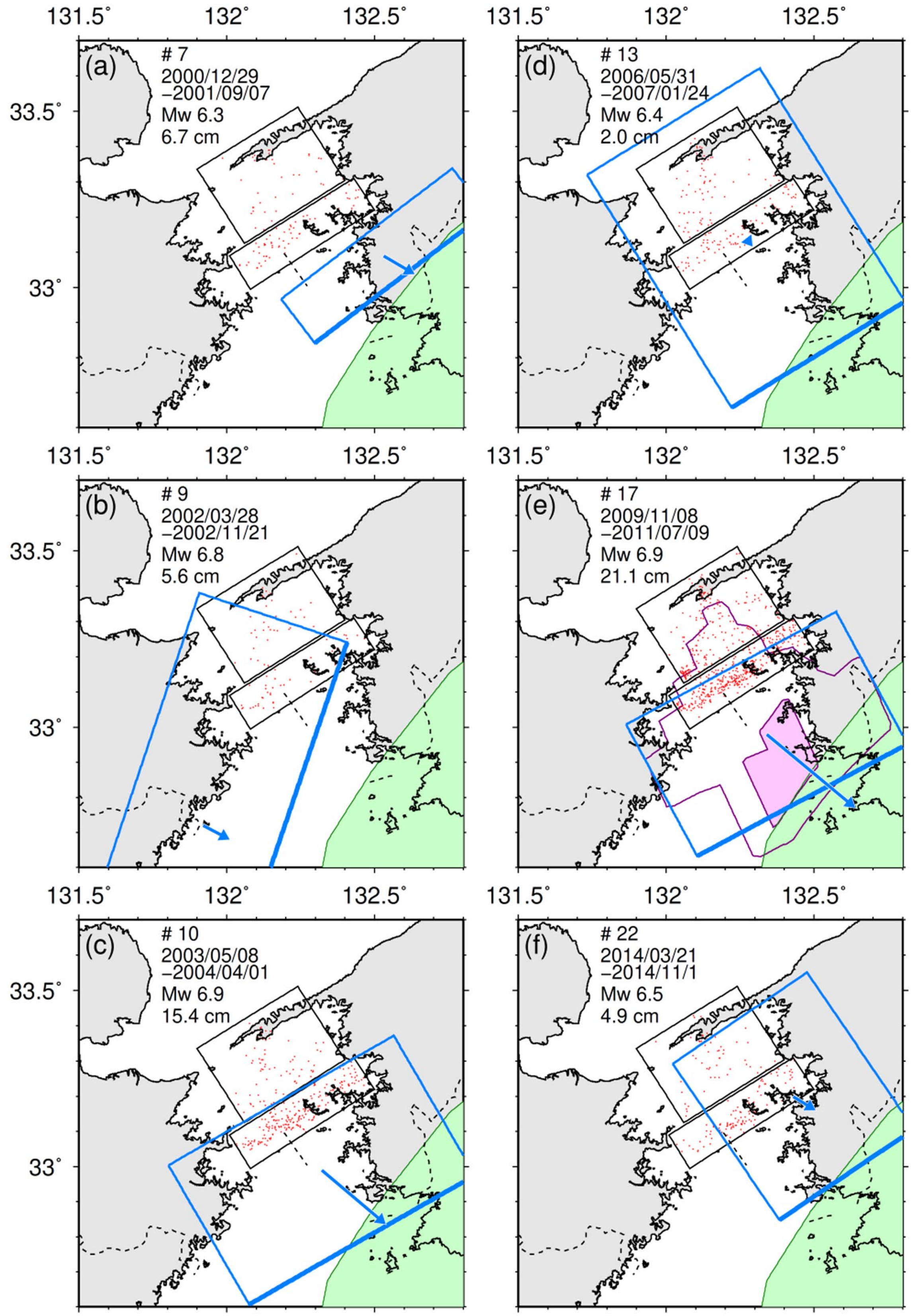

Fig. 6 (See legend on previous page.)

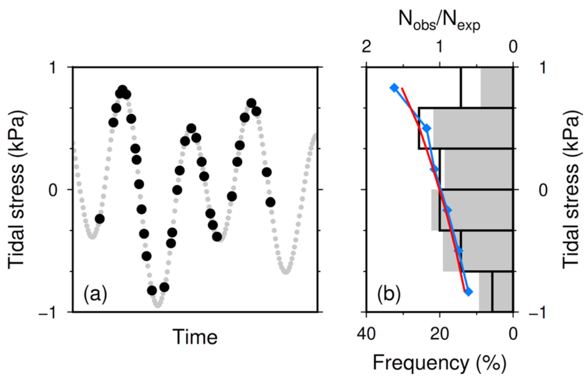

Fig. 7 Example of the tidal sensitivity analysis. **a** Theoretical tidal response (gray circles). Black circles indicate earthquake occurrences. **b** Histogram of tidal stress divided into multiple bins. Gray bars show the distribution of the expected background relative frequency N_{exp} of tidal stress (relative frequency distribution of gray circles in [**a**]), and bars outlined by thick black lines show the distribution of the relative frequency N_{obs} of tidal stress (black circles in [**a**]) at the time of the earthquake (bottom axis). Blue diamonds show the ratio N_{obs}/N_{exp} (top axis). The red line indicates the value obtained by applying the maximum likelihood method (Eq. (1); Yabe et al. 2015) to the N_{obs}/N_{exp} values in the six bins

background region as a unit called a "cluster", and characterized the heterogeneity of friction on the plate interface by the size of the cluster (which determines tremor duration) and the density of the tremor patches (which determines tremor amplitude and energy) and interpreted as follows: shallow tremors contain clusters of short duration and small amplitude (small cluster size, low density) that cannot withstand high stress (i.e., weak patches), resulting in high tidal sensitivity. In contrast, deep tremors occur frequently but last longer (large cluster size), and therefore behave collectively as a large locked area that is less sensitive to stress changes, resulting in low tidal sensitivity.

4.2 Increased tidal sensitivity of DTT during LSSE periods

Figure 10 shows the temporal evolution of the tidal sensitivity α of DTTs for $\Delta\tau$ and $\Delta CFF_{(0.1)}$ calculated for 100 events and shifted by 10 events for clarity. In region Ba (Fig. 10a), α tends to local maxima during LSSE periods, whereas there is no consistent tendency in region Bb (Fig. 10b). The fluttering sensitivity during the Ot 5 period in region Bb is meaningless because it is likely due to the inclusion of noise (see Sect. 2.1). In addition, in cases where the tidal sensitivity is negative, this means that tremors are active when tidal stress suppresses fault slip, which is physically contradictory, and therefore it should be concluded that there is no relationship between tremors and tides.

Here, to verify the reliability of the results of the temporal evolution of the tidal sensitivity, a similar analysis was performed on another DTT catalog (Mizuno and Ide 2019), and the results are shown in Fig. 11. Mizuno and Ide (2019) improved the envelope correlation method to create a tremor catalog with a time resolution of 5 min. The data period was 12.5 years from April 2004 to September 2016, which is approximately half the 22.8 years of the NIED catalog. The tidal sensitivity α was calculated for 500 events and shifted by 50 events. It can be seen that the temporal evolution of the tidal sensitivity shown in Fig. 11 is consistent with the results in Fig. 10.

Figure 12 shows the tidal response of DTTs in region Ba during LSSE periods and other periods (labeled 'Ot'). Comparing all LSSE periods (a, c) with all other periods (b, d), the tidal sensitivity α of DTTs is higher in the former. To test whether the entirety of LSSE periods and the entirety of Ot periods are dominated by periods LSSE 2 and Ot 2, which both contain the most individual events of their respective period types (Fig. 2), we calculated the tidal responses for the same groups excluding LSSE 2 and Ot 2. We found that α for $\Delta CFF_{(0.1)}$ was 0.62 ± 0.15 for LSSEs 1, 3, and 4 combined and 0.26 ± 0.11 for Ot 1, 3, 4, and 5, combined; thus, our initial result that the tidal sensitivity is higher in LSSE periods did not change.

To summarize the above results,

- DTTs in the Bungo Channel depend on $\Delta\tau$ or $\Delta CFF_{(0.1)}$;
- The tidal sensitivity of DTTs in region Ba is higher than that in region Bb, and becomes relatively high during LSSE periods.

Here, we discuss why the tidal sensitivity of DTTs in region Ba, which is at the base of the LSSE area, is particularly high during LSSE periods.

As mentioned in Sect. 4.1, Yabe et al. (2015) characterized the heterogeneity of friction at the plate interface by the size of clusters and the density of tremor patches, and explained that tidal sensitivity is high in smaller, low-density clusters (weak patches). They further pointed out that, as the plate interface weakens, the strength of the velocity-weakening region decreases and tidal sensitivity increases, even in small, high-density clusters.

Because DTTs are often accompanied by SSSEs (Obara 2010), it is assumed that faults are generally weakened (low friction) during DTTs compared to normal periods when SSSEs do not occur. Because fault weakening is correlated with tidal sensitivity (e.g., Rubinstein et al. 2008; Thomas et al. 2009; Houston 2015; Yabe et al. 2015), some tidal sensitivity of DTTs accompanied by SSSEs is observed, even during non-LSSE periods (Fig. 12b, d). Furthermore, because the LSSE area largely includes region Ba (Figs. 1, 6c, e, f), fault weakening in region Ba during LSSE periods is

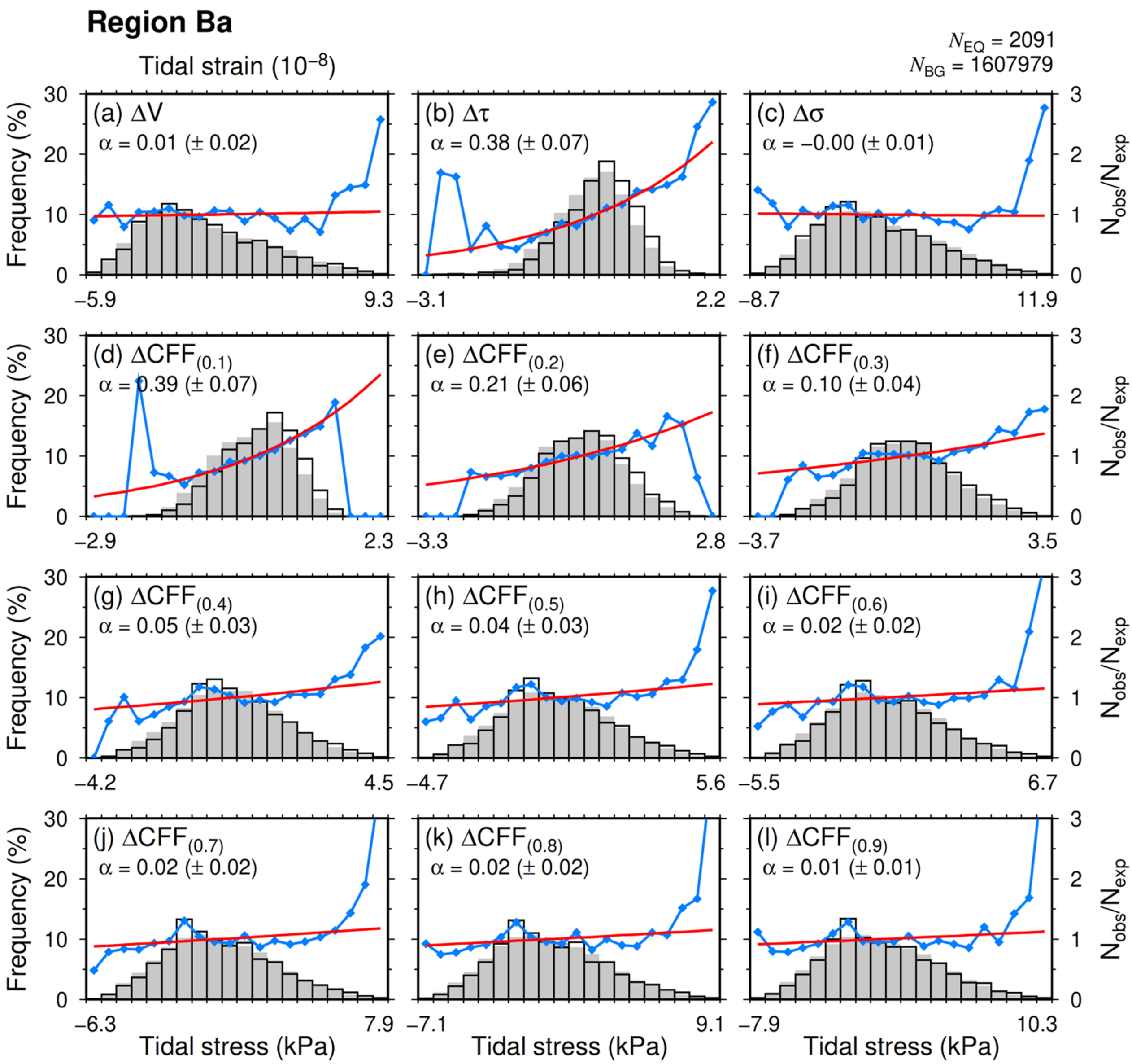

Fig. 8 Tidal sensitivity for each tidal component in region Ba. See Fig. 7b for how to read the figure. The horizontal axis is normalized to the minimum and maximum values of the background data for each component. Values reported in the upper-right part of the figure are the number of DTTs, N_{EQ}, and the background number of events sampled at 15-min intervals during the four days before and after each earthquake, N_{BG} ($N_{BG} = 769 \times N_{EQ}$)

undoubtedly more advanced than during other periods, and region Ba is in a low friction state. As a result, the tidal stress, which is much smaller than the lithostatic stress, more strongly affects the occurrence of DTTs there, causing tidal sensitivity to be higher during LSSE periods than during other periods.

4.3 Differences with previous studies

In this section, we discuss the differences between this and previous studies investigating the relationship between tides and DTTs or background seismicity in southwestern Japan.

Yabe et al. (2015) investigated the relationship between DTTs and tidal shear stress during ETS events in southwest Japan by dividing DTT activity into three periods: "Front", the day on which the number of DTTs per day first exceeded 20; "Initial", the period before the Front; and "Later", the period after the Front. They found that DTTs tended to have higher tidal correlations during the Later period (average 0.41/kPa, compared to 0.33 and

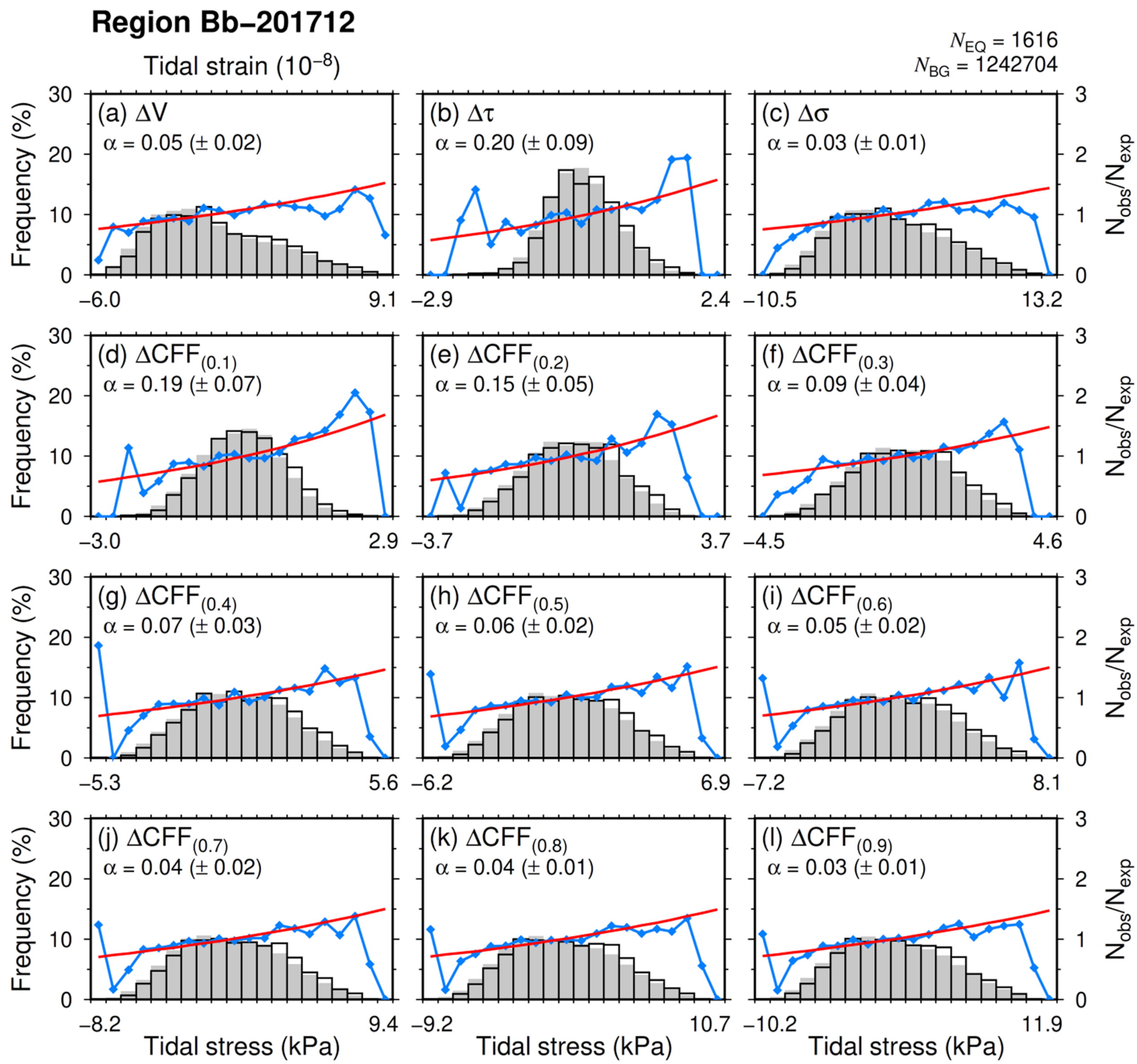

Fig. 9 As Fig. 8, but for region Bb using data up to December 2017

0.08/kPa in the Initial and Front periods, respectively), which they interpreted as resulting from fault weakening during the ETS event. In contrast, we focused herein on the long-term tidal correlation of DTTs, and were not interested in the fine tidal correlation of DTTs in each ETS event; i.e., we investigated the long-term temporal change of the tidal correlation throughout each ETS event. We found that changes in the tidal correlations of $\Delta\tau$ and $\Delta \mathrm{CFF}_{(0.1)}$ in region Ba correspond to the occurrence of LSSEs that affected region Ba. The average tidal sensitivity α is ~0.4 (Fig. 8b, d), but increases to ~0.6 during LSSE periods (Fig. 12a, c) and decreases to ~0.2 during other periods (Fig. 12b, d).

Nakata et al. (2008) discussed the relationship between DTTs and tides using data on hourly DTT durations detected by the automatic tremor monitoring system (ATMOS) (Suda et al. 2009) constructed by Hiroshima University. They explained DTT activity with periods of 12 or 24 h in eastern Shikoku, Japan, by combining periodic stress changes caused by tides and transient increases in stress rate caused by SSSEs. They considered both $\Delta \mathrm{CFF}_{(0.2)}$, i.e., ΔCFF with an apparent friction coefficient $\mu\prime = 0.2$, and its rate $\Delta\left(\Delta \mathrm{CFF}_{(0.2)}\right)$. Because

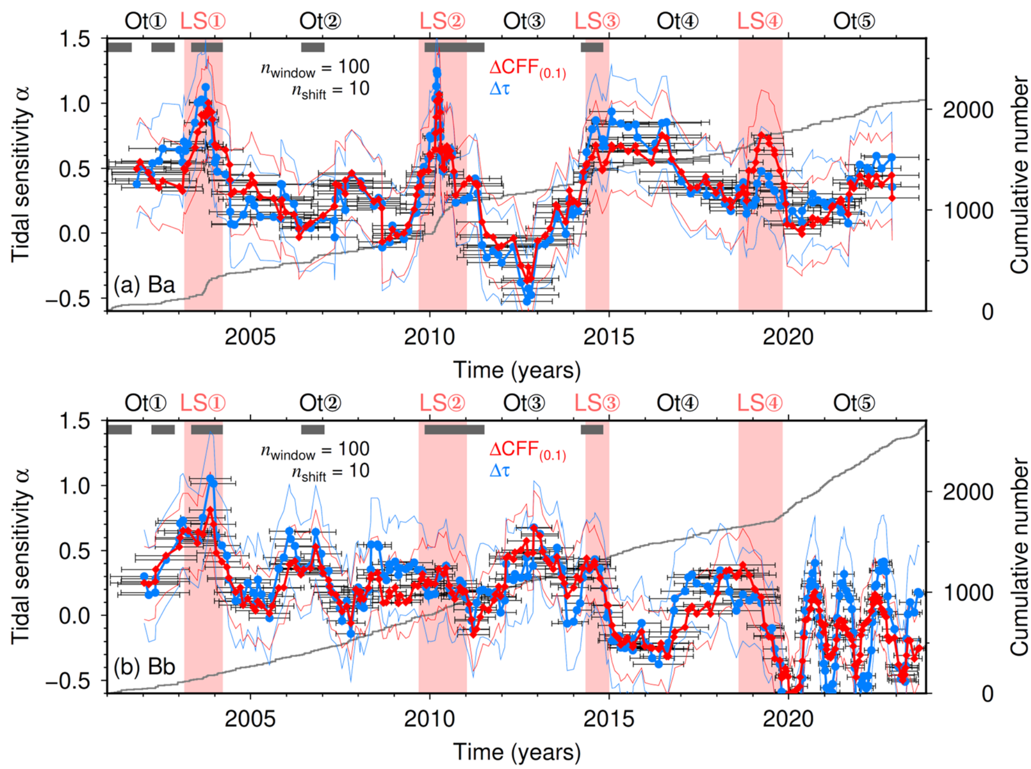

Fig. 10 Temporal changes of α for DTTs considering $\Delta\tau$ and $\Delta CFF_{(0.1)}$. In regions **a** Ba and **b** Bb, the tidal sensitivity α was calculated using windows of $N = 100$ events shifted by 10 events. Horizontal bars indicate the sampling periods. The thick blue and red lines indicate the tidal sensitivity α for $\Delta\tau$ and $\Delta CFF_{(0.1)}$, respectively (left axis). The thin lines indicate the 95% error $\Delta\alpha$. Gray curves indicate the cumulative number of DTTs in each region (right axis). Other symbols are as in Fig. 2

peak DTT activity occurs a few hours *before* the peak in $\Delta CFF_{(0.2)}$, they deemed $\Delta CFF_{(0.2)}$ to be inappropriate as an indicator of DTT occurrence because that violates the law of causality. However, peak DTT activity occurs a few hours *after* the peak in $\Delta\left(\Delta CFF_{(0.2)}\right)$, satisfying causality because the time delay is consistent with the rate- and state-dependent friction law (Dieterich et al. 2000). On the other hand, Houston (2015) proposed a stress threshold failure model in which frictional creep occurs when stress (i.e., secular changes due to plate subduction, transient changes due to SSSEs, and periodic changes due to tides) exceeds the fault strength, immediately generating tectonic tremor. The results of our study suggest that the values of $\Delta\tau$ or $\Delta CFF_{(0.1)}$ themselves may control DTT occurrence, supporting Houston's (2015) hypothesis. Note that this study only focuses on the stress/strain, and does not deny the stress rate theory of Nakata et al. (2008). The relationship between stress rates and DTT will be discussed in another paper.

Tanaka et al. (2015) investigated the relationship between increases and decreases in background seismicity in the Tokai region and LSSE occurrences, taking into account both tides and non-tidal oceanic changes resulting from the Pacific Decadal Oscillation and the Kuroshio Current (large-scale meanders occurred multiple times during 1980–1990 and once in 2004–2005). They found that because the Tokai region is greatly influenced by the large-scale meander of the Kuroshio Current, non-tidal changes are more consistent with the timings of increases and decreases in background seismicity. They also pointed out that LSSEs tend to occur 2–4 years after the peak of long-term stress changes due to tides and non-tidal factors (although it is somewhat difficult to detect a correspondence between long-term stress changes and LSSEs from Fig. 4c of Tanaka et al. 2015). However, the Kuroshio Current has two paths: one runs along the southern coast of Shikoku and Honshu, whereas the other meanders markedly southward off the coast of the Kii Peninsula and Enshu Nada Sea (Kawabe 2003). Both courses convene in the Bungo Channel, which is the target area of the present study, so even if the impact claimed by Tanaka et al. (2015) does exist, the impact of the large-scale meandering of the Kuroshio Current in the present work should be small. Therefore, we did not consider non-tidal oceanographic changes in our study.

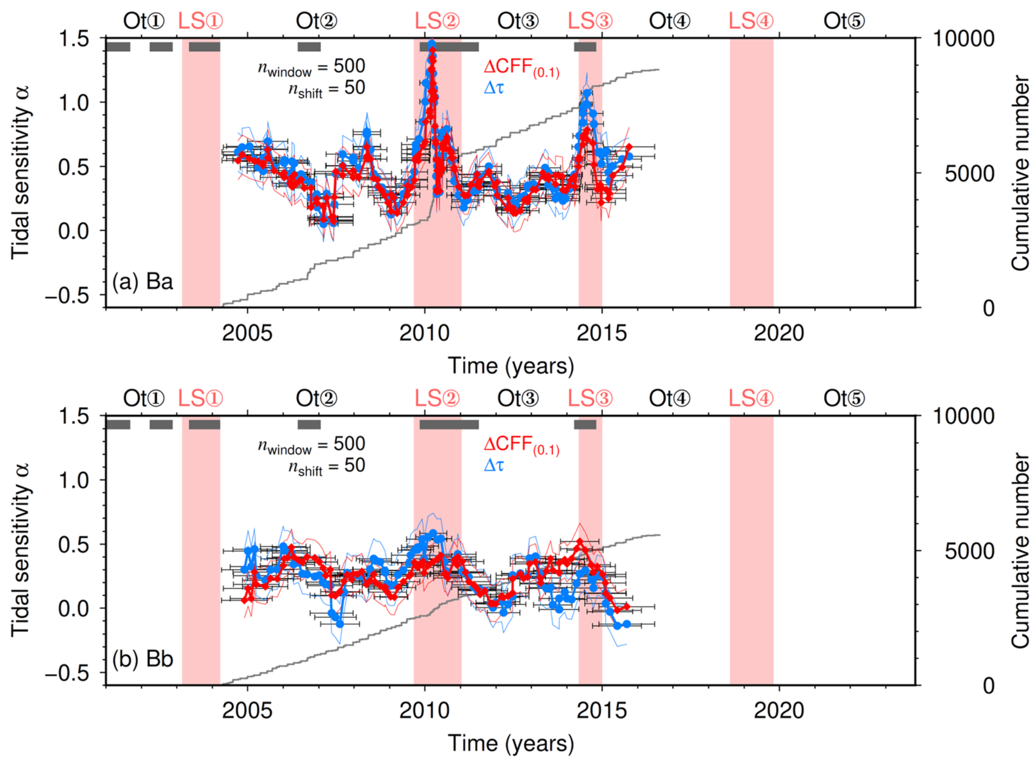

Fig. 11 As Fig. 10, but for tremor catalog by Mizuno and Ide (2019). In regions **a** Ba and **b** Bb, the tidal sensitivity α was calculated using windows of $N = 500$ events shifted by 50 events

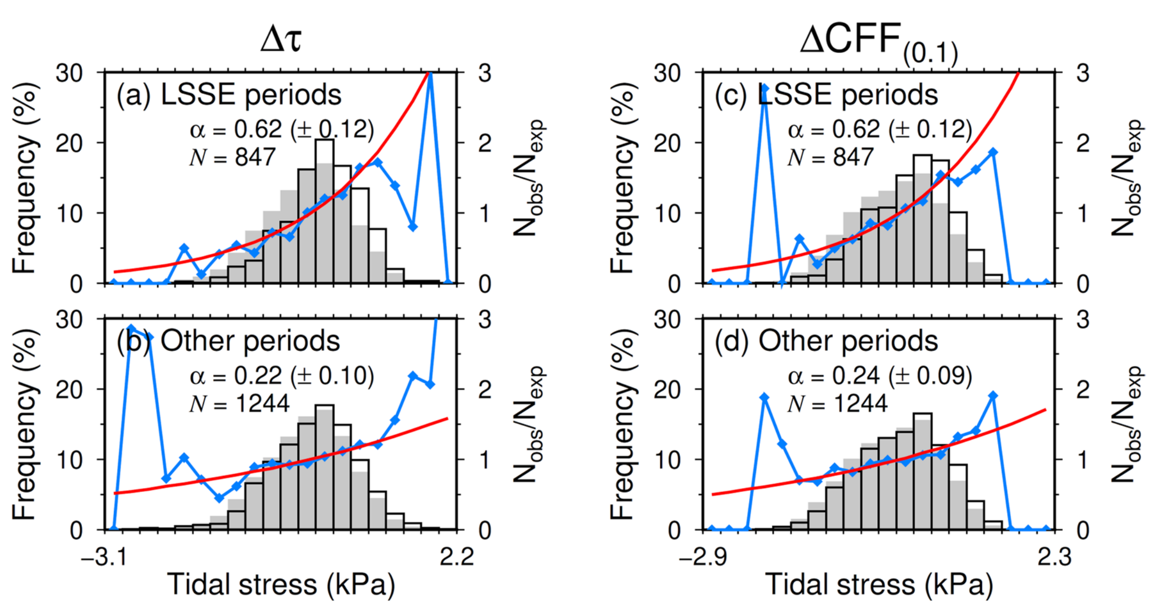

Fig. 12 Tidal stress responses of DTTs in region Ba during LSSE periods and other periods. (Left) $\Delta\tau$, (right) $\Delta CFF_{(0.1)}$. The gray background distributions are those shown in (left) Fig. 8b and (right) Fig. 8d

4.4 Future work

We found that tidal sensitivity generally increased during LSSE periods in region Ba, although the tidal sensitivity of $\Delta\tau$ for LSSE 4 was smaller than that for other LSSE periods (blue line in Fig. 10a). In the Bungo Channel, this difference may simply arise because $\Delta CFF_{(0.1)}$ is more dominant than $\Delta\tau$. However, the tidal (semidiurnal) correlation of TT was reported to have decreased during the 2006 LSSE in Guerrero, Mexico (Peng and Rubin 2017); thus, future work to identify commonalities between the two cases may reveal general patterns.

In the time series of tidal sensitivity α in region Ba (Fig. 10a), a slightly higher tidal sensitivity is apparent for approximately two years after the end of LSSE 3 (~ 2015–2017). In the spatiotemporal distribution of objective LSSE detection (Fig. 5), the correlation coefficient for that 2-year period exceeds 0.6 to the west of 132.4°E, the longitude used as a reference for LSSE occurrence; thus, a small-scale LSSE may have occurred nearby. However, although we corrected for the influence of the 2016 Kumamoto earthquake in advance, associated noise may not have been completely removed. The relationship between the Bungo Channel LSSE (which will likely continue to occur in the future) and the tidal sensitivity of DTTs will become clearer as more cases are recorded.

LSSEs near land can be detected using land-based GNSS stations, but LSSEs in marine areas where GNSS data cannot be obtained in real time are difficult to detect (e.g., Yokota and Ishikawa 2020). Because the tidal correlation of DTTs is sensitive to stress changes caused by LSSEs, it may be possible to detect the occurrence of LSSEs by monitoring the number of tremors and the temporal changes in tidal correlation, which are relatively easy to observe in marine areas. The possibility that LSSEs triggered M_w 7–8 earthquakes has been raised in Mexico (Radiguet et al. 2016) and Chile (Ruiz et al. 2014). If the Bungo Channel LSSE were to trigger a great earthquake along the Nankai Trough in the future, the coupling between plates around the LSSE would be markedly weakened before the earthquake, leading to a high tidal correlation of DTTs. A change in the tidal correlation of DTTs may reflect fault weakening and pore fluid conditions at the plate boundary (e.g., Rubinstein et al. 2008; Thomas et al. 2009; Bartlow et al. 2012; Houston 2015), and is important for considering the temporal evolution of plate coupling during the earthquake cycle.

5 Summary

We investigated the long-term tidal correlation of deep tectonic tremors (DTTs) occurring in the Bungo Channel, southwest Japan. The tidal sensitivity α of DTTs in the shallow side (region Ba) of the DTT occurrence area along the base of the long-term slow slip event (LSSE) area suggests a significant tidal correlation for $\Delta\tau$ and $\Delta CFF_{(0.1)}$; the larger the absolute value of the tidal force, the more likely it is that a DTT will occur or be suppressed. This conclusion is consistent with the findings of previous studies (e.g., Thomas et al. 2009; Houston 2015). The tidal sensitivity of DTTs on the updip side (region Ba) is higher than that on the downdip side (region Bb), in good agreement with the results of earlier works (Ide 2010; Yabe et al. 2015). When the response of DTTs to $\Delta\tau$ and $\Delta CFF_{(0.1)}$ in region Ba was divided into LSSE periods and other periods, DTTs in LSSE periods tended to have higher tidal sensitivity than other periods (although $\Delta\tau$ during LSSE 4 showed less sensitivity). Because region Ba is mostly within the LSSE area, fault coupling in region Ba is smaller during LSSE periods than in other periods. This finding suggests that tidal stress, which is much smaller than lithostatic stress, affects DTT occurrence, thereby increasing tidal sensitivity during LSSE periods compared to other periods.

Abbreviations

AM	Amur continental plate
CFF	Coulomb failure function
DTT	Deep tectonic tremor
ETS	Episodic tremor and slip
GNSS	Global Navigation Satellite System
LSSE or LS	Long-term slow slip event
M_w	Moment magnitude
NIED	National Research Institute for Earth Science and Disaster Resilience
NT	Nankai Trough
OK	Okhotsk plate
Ot	Other
PAC	Pacific plate
PHS	Philippine Sea plate
SSSE	Short-term slow slip event
TT	Tectonic tremor

Acknowledgements
Discussions with the late Dr. Kenji MAEDA were extremely helpful in carrying out this study. The slip distribution data of the 2010 LSSE shown in Fig. 1 were kindly provided by Dr. Ryoko NAKATA. Plate convergence rates were calculated using the Plate Motion Calculator on the UNAVCO website (https://www.unavco.org/). Figures were drawn with Generic Mapping Tools (Wessel et al. 2013). This manuscript was greatly improved by careful reviews of three anonymous reviewers.

Author contributions
HF analyzed the data, wrote most of the manuscript, and made the figures. KA offered suggestions about the organization of the manuscript and helped with manuscript preparation. Both authors read and approved the final manuscript.

Funding
This research was conducted with support from the Japan Meteorological Agency.

Availability of data and materials
The TidalStrain.2 program used to calculate theoretical tidal stresses is available for download from the Meteorological Research Institute repository (https://www.mri-jma.go.jp/Dep/sei/fhirose/research/en.TidalStrain.html). The DTT catalog was obtained from the Earthquake, Tsunami and Volcano Network Center, National Research Institute for Earth Science and Disaster Resilience (https://hinetwww11.bosai.go.jp/auth/tremor/auto_hypo_catal

og). GNSS coordinates were obtained from GEONET F5 solution data analyzed by the Geospatial Information Authority of Japan. The slip distribution data of the SSSE shown in Fig. 1 (Nishimura et al. 2013) and the DTT catalog used in Fig. 11 (Mizuno and Ide 2019) were obtained from the Slow Earthquake Database (Kano et al. 2018; http://www-solid.eps.s.u-tokyo.ac.jp/~sloweq/).

Declarations

Ethics approval and consent to participate
Not applicable.

Consent for publication
Not applicable.

Competing interests
The authors have no competing interests.

Author details
[1]Meteorological Research Institute, Japan Meteorological Agency, 1-1 Nagamine, Tsukuba, Ibaraki 305-0052, Japan. [2]Nagano Local Meteorological Office, Japan Meteorological Agency, 1-8-18 Hakoshimizu, Nagano, Nagano 380-0801, Japan.

Received: 9 August 2024 Accepted: 2 February 2025
Published online: 19 February 2025

References

Bartlow NM, Lockner DA, Beeler NM (2012) Laboratory triggering of stick-slip events by oscillatory loading in the presence of pore fluid with implications for physics of tectonic tremor. J Geophys Res Solid Earth 117:B11411. https://doi.org/10.1029/2012JB009452

Central Disaster Management Council (2003) Report of the specialized investigation committee about Tonankai and Nankai earthquakes (the 16th) (in Japanese). http://www.bousai.go.jp/kaigirep/chuobou/senmon/tounankai_nankaijishin/16/index.html. Accessed 30 Apr 2024

DeMets C, Gordon RG, Argus DF (2010) Geologically current plate motions. Geophys J Int 181:1–80. https://doi.org/10.1111/j.1365-246X.2009.04491.x

Dieterich J, Cayol V, Okubo P (2000) The use of earthquake rate changes as a stress meter at Kilauea volcano. Nature 408:457–460. https://doi.org/10.1038/35044054

Earthquake Research Committee (2013) Long-term evaluation of earthquakes in the Nankai trough, 2nd ed. (in Japanese). http://www.jishin.go.jp/main/chousa/kaikou_pdf/nankai_2.pdf . Accessed 30 Apr 2024

Hirose F, Nakajima J, Hasegawa A (2008) Three-dimensional seismic velocity structure and configuration of the Philippine Sea slab in southwestern Japan estimated by double-difference tomography. J Geophys Res 113:B09315. https://doi.org/10.1029/2007JB005274

Hirose H, Asano Y, Obara K, Kimura T, Matsuzawa T, Tanaka S, Maeda T (2010) Slow earthquakes linked along dip in the Nankai subduction zone. Science 330:1502. https://doi.org/10.1126/science.1197102

Hirose F, Maeda K, Kamigaichi O (2019) Tidal forcing of interplate earthquakes along the Tonga-Kermadec Trench. J Geophys Res 124:10498–10521. https://doi.org/10.1029/2019JB018088

Houston H (2015) Low friction and fault weakening revealed by rising sensitivity of tremor to tidal stress. Nature Geo 8:409–415. https://doi.org/10.1038/ngeo2419

Ide S (2010) Striations, duration, migration and tidal response in deep tremor. Nature 466:356–359. https://doi.org/10.1038/nature09251

Ide S (2012) Variety and spatial heterogeneity of tectonic tremor worldwide. J Geophys Res 117:B03302. https://doi.org/10.1029/2011JB008840

Ide S, Yabe S (2014) Universality of slow earthquakes in the every low frequency band. Geophys Res Lett 41:2786–2793. https://doi.org/10.1002/2014GL059712

Ide S, Yabe S, Tai HJ, Chen KH (2015) Thrust-type focal mechanisms of tectonic tremors in Taiwan: evidence of subduction. Geophys Res Lett 42:3248–3256. https://doi.org/10.1002/2015GL063794

Kano M, Aso N, Matsuzawa T, Ide S, Annoura S, Arai R, Baba S, Bostock M, Chao K, Heki K, Itaba S, Ito Y, Kamaya N, Maeda T, Maury J, Nakamura M, Nishimura T, Obana K, Ohta K, Poiata N, Rousset B, Sugioka H, Takagi R, Takahashi T, Takeo A, Tu Y, Uchida N, Yamashita Y, Obara K (2018) Development of a slow earthquake database. Seism Res Lett 89(4):1566–1575. https://doi.org/10.1785/0220180021

Katakami S, Yamashita Y, Yakiwara H, Shimizu H, Ito Y, Ohta K (2017) Tidal response in shallow tectonic tremors. Geophys Res Lett 44:9699–9706. https://doi.org/10.1002/2017GL074060

Kawabe M (2003) Study on variations of current path and transport of the Kuroshio (in Japanese with English abstract). Oceanogr Jpn 12(3):247–267. https://doi.org/10.5928/kaiyou.12.247

Kobayashi A (2017) Objective detection of long-term slow slip events along the Nankai Trough using GNSS data (1996–2016). Earth Planets Space 69:171. https://doi.org/10.1186/s40623-017-0755-7

Lambert A, Kao H, Rogers G, Courtier N (2009) Correlation of tremor activity with tidal stress in the northern Cascadia subduction zone. J Geophys Res Solid Earth 114:B00A08. https://doi.org/10.1029/2008JB006038

Maeda T, Obara K (2009) Spatio-temporal distribution of seismic energy radiation from low-frequency tremor in western Shikoku, Japan. J Geophys Res 114:B00A09. https://doi.org/10.1029/2008JB006043

Mizuno N, Ide S (2019) Development of a modified envelope correlation method based on maximum-likelihood method and application to detecting and locating deep tectonic tremors in western Japan. Earth Planets Space 71:40. https://doi.org/10.1186/s40623-019-1022-x

Nakajima J, Hasegawa A (2007) Subduction of the Philippine Sea plate beneath southwestern Japan: slab geometry and its relationship to arc magmatism. J Geophys Res 112:B08306. https://doi.org/10.1029/2006JB004770

Nakata R, Suda N, Tsuruoka H (2008) Non-volcanic tremor resulting from the combined effect of Earth tides and slow slip events. Nature Geo 1:676–678. https://doi.org/10.1038/ngeo288

Nakata R, Hino H, Kuwatani T, Yoshida S, Okada M, Hori T (2017) Discontinuous boundaries of slow slip events beneath the Bungo Channel, southwest Japan. Sci Rep 7:6129. https://doi.org/10.1038/s41598-017-06185-0

National Research Institute for Earth Science and Disaster Resilience (2019) 340th Earthquake Research Committee documents. 17.

Nishimura T, Matsuzawa T, Obara K (2013) Detection of short-term slow slip events along the Nankai Trough, southwest Japan, using GNSS data. J Geophys Res Solid Earth 118:3112–3125. https://doi.org/10.1002/jgrb.50222

Obara K (2002) Nonvolcanic deep tremor associated with subduction in southwest Japan. Science 296:1679–1681. https://doi.org/10.1126/science.1070378

Obara K (2010) Phenomenology of deep slow earthquake family in southwest Japan: spatiotemporal characteristics and segmentation. J Geophys Res 115:B0025. https://doi.org/10.1029/2008JB006048

Obara K, Kato A (2016) Connecting slow earthquakes to huge earthquakes. Science 353:253–257. https://doi.org/10.1126/science.aaf1512

Obara K, Tanaka S, Maeda T, Matsuzawa T (2010) Depth-dependent activity of non-volcanic tremor in southwest Japan. Geophys Res Lett 37:L13306. https://doi.org/10.1029/2010GL043679

Ozawa S (2017) Long-term slow slip events along the Nankai trough subduction zone after the 2011 Tohoku earthquake in Japan. Earth Planets Space 69:56. https://doi.org/10.1186/s40623-017-0640-4

Ozawa S, Kawabata R, Kokado K, Yarai H (2020) Long-term slow slip events along the Nankai trough delayed by the 2016 Kumamoto earthquake, Japan. Earth Planets Space 72:61. https://doi.org/10.1186/s40623-020-01189-z

Peng Y, Rubin AM (2017) Intermittent tremor migrations beneath Guerrero, Mexico, and implications for fault healing within the slow slip zone. Geophys Res Lett 44:760–770. https://doi.org/10.1002/2016GL071614

Radiguet M, Pefettini M, Cotte N, Gualandi A, Valette B, Kostoglodov V, Lhomme T, Walpersdorf A, Cabral-Cano E, Campillo M (2016) Triggering of the 2014 M_w7.3 Papanoa earthquake by a slow slip event in Guerrero, Mexico. Nat Geo 9:829–834. https://doi.org/10.1038/NGEO2817

Rogers G, Dragert H (2003) Episodic tremor and slip on the Cascadia subduction zone: the chatter of silent slip. Science 300:1942–1943. https://doi.org/10.1126/science.1084783

Rubinstein JL, La Rocca M, Vidale JE, Creager KC, Wech AG (2008) Tidal modulation of nonvolcanic tremor. Science 319:186–189. https://doi.org/10.1126/science.1150558

Ruiz S, Metois M, Fuenzalida A, Ruiz J, Leyton F, Grandin R, Vigny C, Madariaga R, Campos J (2014) Intense foreshocks and a slow slip event preceded the 2014 Iquique M_w 8.1 earthquake. Science 345:1165–1169. https://doi.org/10.1126/science.1256074
Suda N, Nakata R, Kusumi T (2009) An automatic monitoring system for non-volcanic tremors in southwest Japan. J Geophys Res 114:B00A10. https://doi.org/10.1029/2008JB006060
Takagi R, Uchida N, Obara K (2019) Along-strike variation and migration of long-term slow slip events in the western Nankai subduction zone, Japan. J Geophys Res 124:3853–3880. https://doi.org/10.1029/2018JB016738
Tanaka Y, Yabe S, Ide S (2015) An estimate of tidal and non-tidal modulations of plate subduction speed in the transition zone in the Tokai district. Earth Planets Space 67:141. https://doi.org/10.1186/s40623-015-0311-2
Thomas AM, Nadeau RM, Bürgmann R (2009) Tremor-tide correlations and near-lithostatic pore pressure on the deep San Andreas fault. Nature 462:1048–1051. https://doi.org/10.1038/nature08654
Wessel P, Smith WHF, Scharroo R, Luis J, Wobbe F (2013) Generic mapping tools: improved version released. Eos Trans AGU 94:409–410. https://doi.org/10.1002/2013EO450001
Yabe S, Tanaka Y, Houston H, Ide S (2015) Tidal sensitivity of tectonic tremors in Nankai and Cascadia subduction zones. J Geophys Res 120:7587–7605. https://doi.org/10.1002/2015JB012250
Yokota Y, Ishikawa T (2020) Shallow slow slip events along the Nankai Trough detected by GNSS-A. Sci Adv 6(3):eaay5786. https://doi.org/10.1126/sciadv.aay5786